JACS
JOURNAL OF THE AMERICAN CHEMICAL SOCIETY
pubs.acs.org/JACS
Article

Rational Functionalization of a C_{70} Buckybowl To Enable a C_{70}:Buckybowl Cocrystal for Organic Semiconductor Applications

Guangpeng Gao,[⊥] Meng Chen,[⊥] Josiah Roberts, Meng Feng, Chengyi Xiao, Guowei Zhang, Sean Parkin, Chad Risko, and Lei Zhang*

Cite This: J. Am. Chem. Soc. 2020, 142, 2460−2470

ABSTRACT: Fullerene fragments, referred to as buckybowls, are garnering interest due to their distinctive molecular shapes and optoelectronic properties. Here, we report the synthesis and characterization of a novel C_{70} subunit, diindeno[4,3,2,1-*fghi*:4′,3′,2′,1′-*opqr*]perylene, that is substituted with either triethylsilyl(TES)-ethynyl or 2,4,6-triisopropylphenyl groups at the *meta*-positions. The resulting compounds (**1** and **2**) display a bowl-to-bowl inversion at room temperature. Notably, the substituent groups on the *meta*-positions alter both the geometric and the electronic properties as well as the crystal packing of the buckybowls. In contrast to the 2,4,6-triisopropylphenyl groups in **2**, the TES-ethynyl groups in **1** lead to enhanced bond length alternation, resulting in weaker aromaticity of the six-membered rings of the buckybowl skeleton. **1** forms one-dimensional (1D) concave-in-convex stacking columns, and when **1** is blended with C_{70}, the buckybowls encapsulate C_{70} and result in two-dimensional cocrystals. Organic field-effect transistor (OFET) measurements demonstrate that **1** displays a hole mobility of 0.31 $cm^2\ V^{-1}\ s^{-1}$, and the **1**-C_{70} cocrystal exhibits ambipolar transport characteristics with electron and hole mobilities approaching 0.40 and 0.07 $cm^2\ V^{-1}\ s^{-1}$, respectively. This work demonstrates the potential of buckybowls for the development of organic semiconductors.

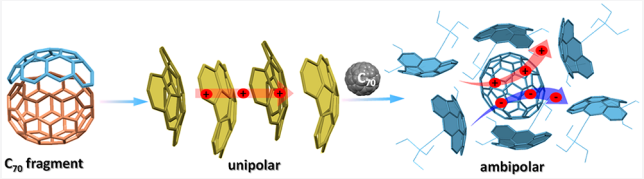

INTRODUCTION

The synthesis of bowl-shaped polycyclic aromatic hydrocarbons (PAHs), so-called buckybowls or π-bowls, is accomplished by incorporating five-membered rings into sp^2 hybridized hexagonal networks.[1] These curved structures, which can be considered as subunits of C_{60} and C_{70}, are likely to provide a variety of distinctive properties, such as chiroptical activities, dynamic inversion behavior, and supramolecular assemblies.[2] Among the applications suggested for buckybowls, their use in organic semiconductors is particularly promising,[3] as the buckybowls provide novel routes to control and optimize molecular packing in the solid,[4] distinct electronic, photophysical, and redox properties, and the formation of complexes with the corresponding fullerenes due to their shape complementarity.[5] Several reports have shown that tuning of the crystal packing of corannulene derivatives can significantly alter the electronic properties of the materials that lead to charge-carrier mobilities of more than $10^{-2}\ cm^2\ V^{-1}\ s^{-1}$.[3c−e] Recently, Hu and co-workers successfully demonstrated the preparation of one-dimensional cocrystals of corannulene and C_{60} by a solution process, with the cocrystal exhibiting electron mobilities up to 0.11 $cm^2\ V^{-1}\ s^{-1}$ and a photoresponse of 0.09 A W^{-1}.[6] Further, these molecular materials demonstrate high stability and solubility and are less prone to aggregation than their flat PAH counterparts, features that are critical for solution-processed materials.[7]

To take advantage of the physical and chemical properties offered by buckybowls, new synthetic methods need to be developed to enable the creation of buckybowls with prescribed shape and functionality. Currently, however, there are no general synthetic routes to these buckybowls, and only a few synthetic pathways exist to create them, for example, flash vacuum pyrolysis (FVP)[1c] and solution-phase synthesis.[8] Although FVP has been extensively used to prepare highly strained buckybowls, FVP suffers from low yields, leads to undesired rearrangement of the molecular framework at high temperatures, and has limited functional group tolerance.[1c] By contrast, solution-phase syntheses are able to prepare buckybowls with a wide array of functional groups under mild conditions.[9] This strategy usually involves palladium-catalyzed intramolecular C−H arylation to form five-/six-membered rings and is one of the most promising strategies for obtaining buckybowls to date.[9,10] The groups of Scott,[11] Müllen,[12] and Tai,[13] for instance, have successfully demonstrated the utilization of palladium-catalyzed C−C bond formation reactions to subunits of fullerenes. However, this strategy is less efficient for highly strained buckybowls and

Received: November 12, 2019
Published: January 3, 2020

https://dx.doi.org/10.1021/jacs.9b12192
J. Am. Chem. Soc. 2020, 142, 2460−2470

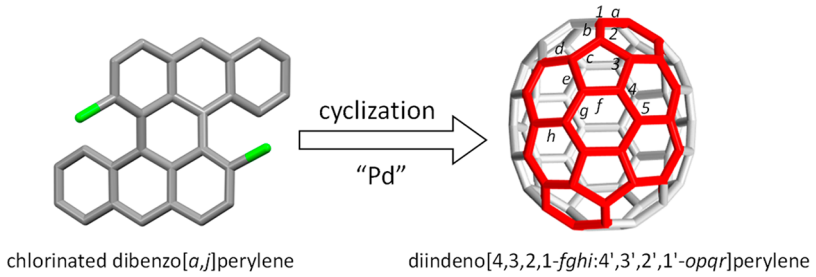

Figure 1. Chlorinated dibenzo[*a,j*]perylene and diindeno[4,3,2,1-*fghi*:4′,3′,2′,1′-*opqr*]perylene mapped onto C_{70} that contains five types of carbon atoms (labeled 1−5) and eight types of C−C bonds (label *a*−*h*).

Scheme 1. Synthetic Steps to the Functionalized Diindeno[4,3,2,1-*fghi*:4′,3′,2′,1′-*opqr*]perylenes 1 and 2

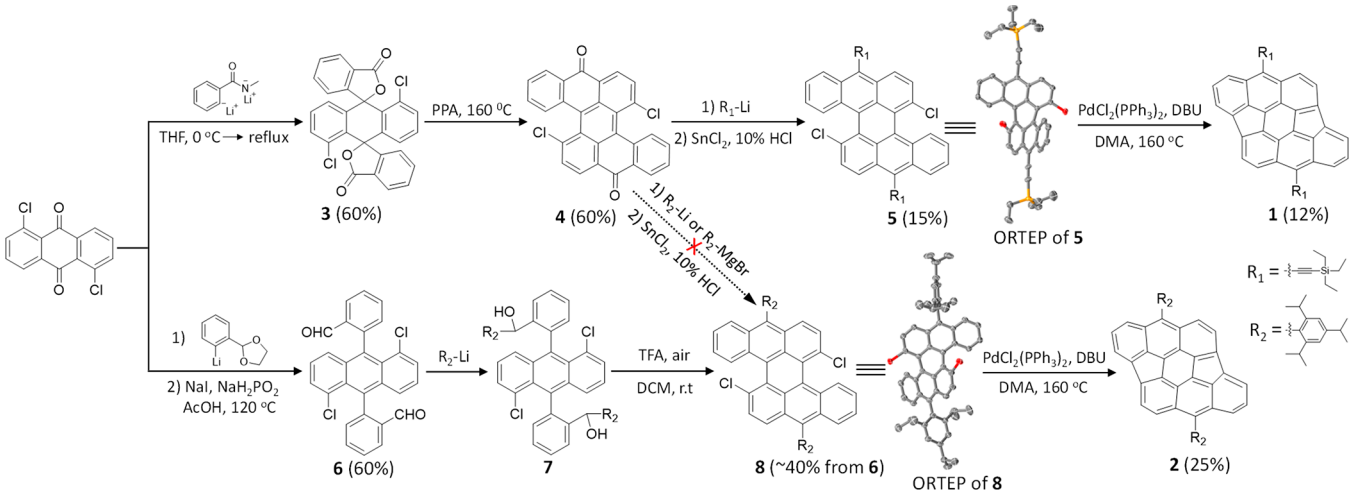

typically requires the careful preinstallation of halide groups onto the precursors.[10] Therefore, generation of buckybowls remains a considerable synthetic challenge, especially for C_{70} fragments,[14] due to the considerable strain involved, and consequently their applications in organic devices are underexplored.[15]

By contrast with the more well-studied subunits of C_{60}, the subunits of C_{70} may provide new fundamental insight into fullerene chemistry and act as models to understand the electronic properties of C_{70}; notably, fragments for even higher-numbered fullerenes remain elusive.[16] Using palladium-catalyzed arylation reactions, we report the synthesis and characterization of *meta*-functionalized diindeno[4,3,2,1-*fghi*:4′,3′,2′,1′-*opqr*]perylenes by palladium-catalyzed intramolecular C−H arylation of chlorinated dibenzo[*a,j*]perylenes (Figure 1). The diindeno[4,3,2,1-*fghi*:4′,3′,2′,1′-*opqr*]perylene scaffold is a new subunit of C_{70} and other higher fullerenes (C_{76}, C_{78}, and C_{84}), which contains all carbon atom types (labeled 1−5) and C−C bonds (labeled *a*−*h*) present in C_{70}. The buckybowl skeleton was functionalized at the *meta*-positions with triethylsilyl-ethynyl (TES-ethynyl) (**1**) and 2,4,6-triisopropylphenyl (**2**) to ensure solubility and stability and to tune the crystal packing in the solid state. We discuss in detail the synthetic approach, solution and solid-state structures, electronic structures, and charge-carrier transport properties of **1** and **2** through a combination of experimental and computational results. It is found that the electronic properties and crystal packing of **1** and **2** are greatly influenced by the substituents, with **1** behaving as a p-type organic semiconductor with mobilities up to 0.31 $cm^2\ V^{-1}\ s^{-1}$. Moreover, **1** is capable of coassembly with C_{70} to form two-dimensional cocrystals, which exhibit ambipolar transport characteristics with electron and hole mobilities up to 0.40 and 0.07 $cm^2\ V^{-1}\ s^{-1}$, respectively.

RESULTS AND DISCUSSION

Synthesis. Scheme 1 shows the synthesis of functionalized diindeno[4,3,2,1-*fghi*:4′,3′,2′,1′-*opqr*]perylenes **1** and **2**. Our synthetic protocol relies on the palladium-catalyzed intramolecular C−H arylation of chlorinated dibenzo[*a,j*]perylenes **5** and **8**, which are the key intermediate compounds. To access TES-ethynyl-functionalized dibenzo[*a,j*]perylene **5**, we chose 1,5-dichloroanthraquinone as the starting material. Double condensation of 1,5-dichloroanthraquinone with dilithiated *N*-methylbenzamide provided dilactone **3** in 60% yield, which could be readily rearranged to diketone **4** in polyphosphoric acid (PPA). A subsequent nucleophilic addition between **4** and lithium TES-acetylide provided the alcohol, which was followed by reductive aromatization with $SnCl_2$/HCl to form the desired intermediate **5** in 15% yield. Our initial attempt to prepare 2,4,6-triisopropylphenyl-functionalized dibenzo[*a,j*]-perylenes **8** via another nucleophilic addition reaction between diketone **4** and 2,4,6-triisopropylphenyllithium or Grignard reagent (R_2−Li or R_2−MgBr) as the nucleophile led to complex mixtures and no desired **8** present. Alternatively, we developed a three-step pathway to compound **8**. Treatment of 1,5-dichloroanthraquinone with lithiated 2-(2-bromophenyl)-1,3-dioxolane followed by reductive aromatization with NaI/NaH_2PO_2 in acetic acid (AcOH) afforded dialdehyde **6** in 60% yield. Subsequently, the addition of 2,4,6-triisopropylphenyllithium to **6** followed by treatment of diol **7** with trifluoroacetic

https://dx.doi.org/10.1021/jacs.9b12192
J. Am. Chem. Soc. 2020, 142, 2460−2470

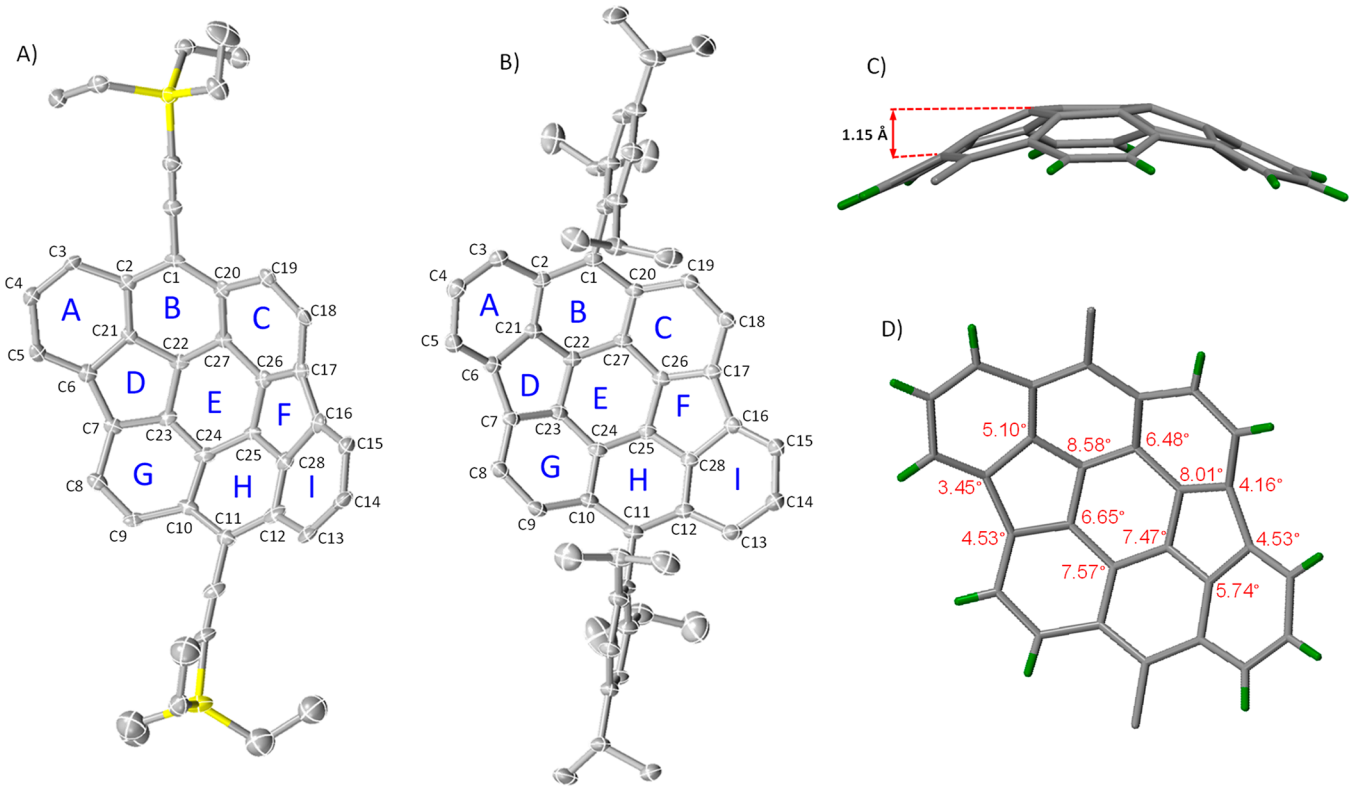

Figure 2. Ellipsoid plots of **1** (A) and **2** (B) with 30% probability ellipsoids; side view (C) and POAV pyramidalization angles (D) of **1** (TES-ethynyl groups are omitted for clarity).

acid (TFA) under air resulted in the formation of compound **8** in 40% yield. Both **5** and **8** were further confirmed by X-ray diffraction analysis. Finally, the intermediates **5** and **8** were converted into **1** in 12% yield and **2** in 25% yield via the palladium-catalyzed intramolecular C−H arylation with $PdCl_2(PPh_3)_2$ as catalyst and 1,8-diazabicyclo[5.4.0]undec-7-ene (DBU) as base in dimethylacetamide (DMA) at 160 °C. Compounds **1** and **2** are soluble in common solvents and unambiguously verified by spectroscopic analysis and their X-ray crystal structures.

X-ray Crystallography. Single crystals of **1** and **2** suitable for X-ray diffraction analysis were grown by slow diffusion of methanol into toluene at room temperature. As shown in Figure 2, the two compounds adopt bowl-shaped structures, with bowl depths of 1.15 Å, here defined as the perpendicular distance between the plane of the central six-membered rings and the main plane containing the four carbon atoms labeled C2, C9, C12, and C19 in Figure 2C. This value is comparable to that of sumanene (1.1 Å) and is significantly larger than that of corannulene (0.88 Å)[17] and dicyclopenta[4,3,2,1-*ghi*:4′,3′,2′,1′-*pqr*]perylene (0.89 Å).[18] The degrees of curvature of **1** and **2** were quantitatively evaluated by π-orbital axis vector analysis (POAV). The POAV angles of the central six-membered rings in **1** and **2** are in the range of 6.3−8.6°. The maximum POAV pyramidalization angles are estimated to be 8.6° for **1** and 8.5° for **2** at the C22 positions, values that are close to that of corannulene (9.1°).[5f] We observe that the pendant TES-ethynyl and 2,4,6-triisopropylphenyl groups influence the bond length alternation pattern of the buckybowl. In contrast to the TES-ethynyl groups of **1**, the 2,4,6-triisopropylphenyl groups of **2** are nearly perpendicular to the rings labeled B and E (Figure 2B). The C6−C7 and C16−C17 bond lengths in **1** are 1.487 and 1.469 Å, which are close to that of the single bond among the sp^2-hybridized carbon atoms (1.470−1.480 Å) (Table 1). These same bonds in **2** are elongated to 1.508 and 1.505 Å, respectively, which minimizes the aromatic character of rings D and F. In addition, the C3−

Table 1. Selected Bond Lengths from the X-ray Crystallographically Determined Molecular Structures and Calculated HOMA Values for 1 and 2

	1	2
Bond Length[a]		
C2−C3	1.461	1.431
C3−C4	1.341	1.368
C6−C7	1.487	1.508
C12−C13	1.465	1.433
C13−C14	1.350	1.366
C16−C17	1.469	1.505
C17−C18	1.443	1.426
HOMA[b]		
ring A	0.42	0.67
ring B	0.87	0.80
ring C	0.34	0.69
ring D	0.26	−0.01
ring E	0.52	0.76
ring F	0.15	0.01
ring G	0.47	0.70
ring H	0.60	0.74
ring I	0.28	0.62

[a]Selected experimental bond lengths. [b]HOMA values were calculated by using the normalization constant of 257.7 and the optimal bond length of 1.388 Å.

https://dx.doi.org/10.1021/jacs.9b12192
J. Am. Chem. Soc. 2020, 142, 2460−2470

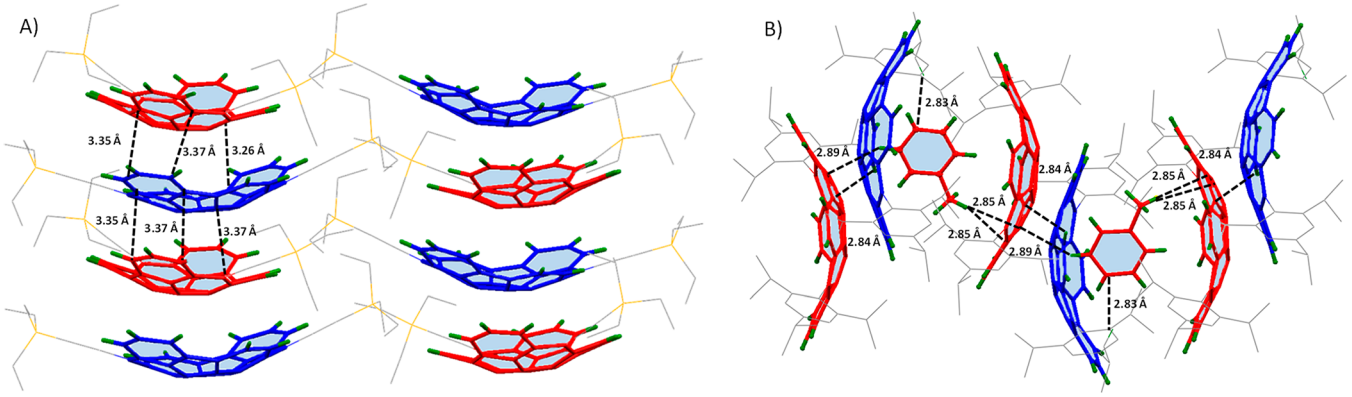

Figure 3. Molecular packing of **1** (A) and **2** (B) showing close contact distances (*M,M*-enantiomers are in red, and *P,P*-enantiomers are in blue).

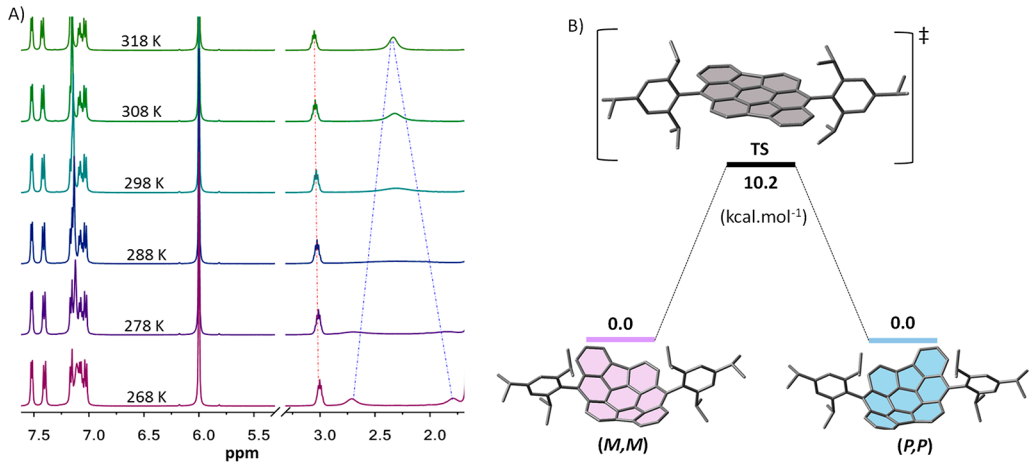

Figure 4. (A) Variable-temperature ^{1}H NMR spectra of **2** in 1,1,2,2-tetrachloroethane-d_2 and (B) calculated diagram for the bowl inversion process of **2**.

C4 and C13−C14 in **1** are relatively short, with lengths of 1.341 and 1.350 Å, indicating a high degree of double bond character; these bond lengths suggest that the π electrons are quite localized. Whereas the C2−C3, C12−C13, and C17−C18 in **1** are unusually long for aromatic C−C double bonds, with bond lengths in the range of 1.443−1.465 Å, these same bonds in **2** range between 1.366 and 1.437 Å, which fall within the typical C═C bond values for polycyclic aromatic hydrocarbons (1.4 ± 0.04 Å). Thus, the TES-ethynyl groups decrease the aromaticity of the six-membered rings of the buckybowl skeleton.

To gain deeper insight into the aromatic character of the compounds, we carried out harmonic oscillator model of aromaticity (HOMA)[19] analyses on **1** and **2** (Table 1). The five-membered rings (D and F) in **1** have small HOMA values (0.26 and 0.15, respectively), consistent with strong bond length alternation and weak aromaticity. The HOMA values of the five-membered rings in **2** are close to zero, indicating the two rings can be considered to be nonaromatic that partially break the conjugation. On the other hand, the six-membered ring B in **1** has the highest value of 0.87, ring H has a value of 0.60, while rings A, C, E, G, and I have HOMA values lower than 0.54. In contrast, the six-membered rings in **2** have HOMA values higher than 0.60, and ring B has the highest value of 0.80, indicating stronger aromatization. The enhancement of aromaticity of the six-membered rings in **2** relative to **1** correlates well with the considerably reduced C−C bond length alternations in **2** as compared to **1**.

As shown in Figure 3, **1** and **2** crystallize as racemic mixtures of chiral bowls, with *P,P*- and *M,M*-enantiomers in the crystals. **1** crystallizes in the $Pca2_1$ space group with four molecules per unit cell. The *P,P*- and *M,M*-enantiomers form a one-dimensional (1-D) concave-in-convex stacking column with the TES-ethynyl groups in adjacent enantiomers alternating by a rotation angle of 45° to alleviate the steric hindrance of the bulky TES groups (Figure 3A). The multiple short C−C contacts among adjacent enantiomers are in the range of 3.26−3.37 Å within a given stack, which are shorter than the sum of the van der Waals radii of the two carbons (3.40 Å). Notably, the bowl-stacking direction in adjacent stacks is the same, likely resulting in the dipole moments in the crystals.[5d] However, introducing the bulkier 2,4,6-triisopropylphenyl substituent in **2** does not allow for that same concave-in-convex stacking found in **1**. Compound **2** crystallizes in the $P2_1/c$ space group with eight molecules per unit cell. The packing arrangement of **2** contains slipped dimer structures, which are involved in short C−H···π contacts (2.84 Å) between the curved π-surfaces of the *P,P*- and *M,M*-enantiomers (Figure 3B). It also contains a slipped-stacked columnar arrangement with toluene solvent molecules situated in the voids among the adjacent molecules, which interact mainly via C−H···π contacts (2.85 and 2.89 Å) with curved π-surfaces to stabilize the crystal network. The packing difference between **1** and **2** is likely due to the iso-

https://dx.doi.org/10.1021/jacs.9b12192
J. Am. Chem. Soc. 2020, 142, 2460−2470

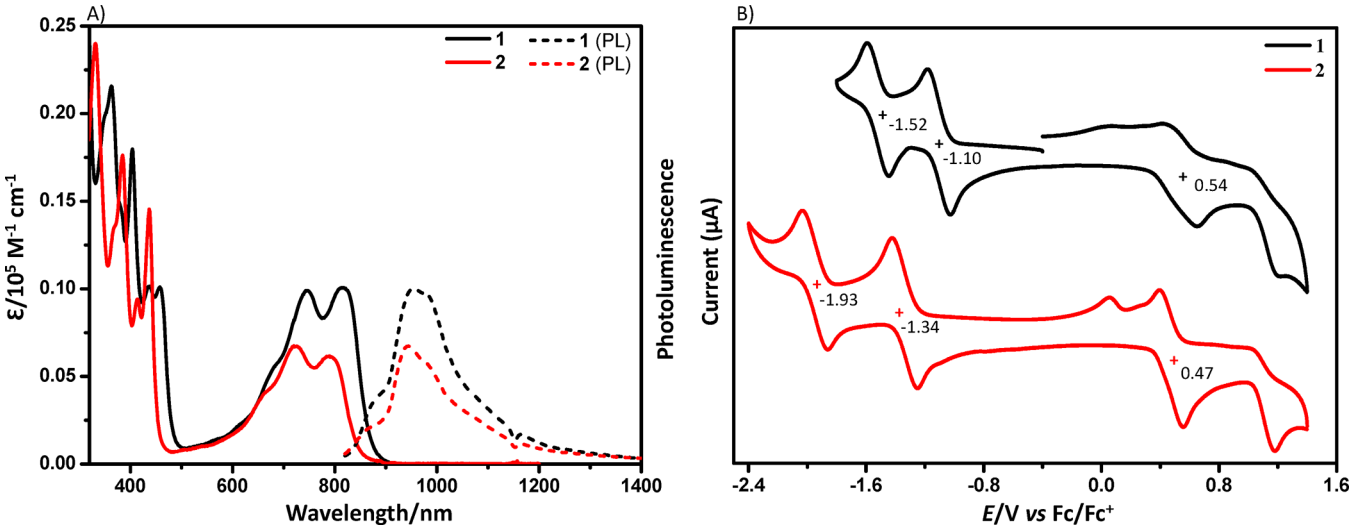

Figure 5. (A) UV/vis absorption (solid line) and photoluminescence spectra (dotted line) of **1** and **2** in chloroform (~10^{-5} M) and (B) cyclic voltammograms of **1** and **2**. The CV experiments were performed in nitrogen-purged dichloromethane with tetrabutylammonium hexafluorophosphate ($TBAPF_6$, 0.1 M) as the supporting electrolyte, with a scan rate of 100 mV/s.

Table 2. Photophysical Properties and Electrochemical Data for 1 and 2

	UV−vis[a]			CV[c]				
	λ_{max} (nm)	ε_{max} (M^{-1} cm^{-1})	λ_{emi} (nm)[b]	$E_{1/2}^{red}$ (V)	$E_{1/2}^{ox}$ (V)	EA (eV)	IP (eV)	E_g^{opt} (eV)
1	747/818	9899/10066	952	−1.10, −1.52	0.54	−3.76	−5.15	1.41
2	720/790	6745/6164	941	−1.34, −1.93	0.47	−3.55	−5.16	1.46

[a]The photophysical properties of the compounds were measured in $CHCl_3$ (10^{-5} M). [b]Measured in dilute $CHCl_3$ solution. [c]CVs were measured in dichloromethane with tetrabutylammonium hexafluorophosphate ($TBAPF_6$, 0.1 M) as the supporting electrolyte with a scan rate of 100 mv/s; $E_{1/2}^{ox}$ and $E_{1/2}^{red}$ are half-wave potentials of the oxidative and reductive waves (vs Fc/Fc^+); EA and IP values were calculated from the onset of the first reduction and oxidation peaks, respectively; and E_g^{opt} is the optical band gap and is estimated from the onset of the absorption peak.

propyl groups of **2** that partially occupy volume between the adjacent bowls to fulfill the requirement for the concave-in-convex stacking through $\pi-\pi$ interactions.

Conformational Dynamics. The potential for a bowl-to-bowl inversion of **2** was investigated by variable-temperature ^{1}H NMR spectroscopy. The ^{1}H NMR spectrum of **2** in 1,1,2,2-tetrachloroethane-d_2 at 268 K exhibits three peaks for −CH− protons of isopropyl groups at δ = 3.01, 2.71, and 1.79 ppm, which indicate that there is no bowl-to-bowl inversion at this temperature (Figure 4A). As the temperature increased, the two peaks at 2.71 and 1.79 ppm are gradually broadened and finally coalesce at 288 K. Fitting the data by using the Eyring equation[20] gives the thermodynamic parameters $\Delta H^{\ddagger}$ of 83 ± 2 kJ/mol and $\Delta S^{\ddagger}$ of 102 ± 6 J/(mol·K) (Figure S12). Accordingly, the bowl-to-bowl inversion energy ($\Delta G^{\ddagger}$) is determined to be 12.9 ± 0.9 kcal mol^{-1} at a coalescence temperature of 288 K. The inversion energy was also evaluated via density functional theory (DFT) calculations at the B3LYP/cc-pVDZ level of theory (see details in the Supporting Information). The DFT calculations reveal that the inversion of **2** proceeds via a planar transition state, with an inversion barrier of 10.2 kcal mol^{-1}, a value in good agreement with the experimental value (Figure 4B). This result is also consistent with the observation of *P,P*- and *M,M*-enantiomers' coexistence in the crystals.

Electronic Structure, Optical, and Redox Properties. We begin with a description of the electronic structures of **1** and **2**, as described by DFT calculations at the optimally tuned (OT)-LC-ωHPBE/cc-pVDZ+GD3 level of theory. The calculations were carried out using the *Gaussian 16* software suite,[21] and the tuned ω values may be found in the Supporting Information. For the highest-occupied molecular orbitals (HOMO), the ethynyl group on the substituent in **1** does lead to a more delocalized wave function, which results in a slight (0.03 eV) stabilization of the HOMO in **1** (−6.18 eV) when compared to that of **2** (−6.15 eV). Likewise, the lowest-unoccupied molecular orbital (LUMO) in **1** delocalizes from the buckybowl onto the ethynyl moieties; here, the LUMO is 0.2 eV stabilized in **1** (−2.14 eV) when compared to **2** (−1.94 eV) (Table S2). These variations in the molecular orbital portend differences that may be expected in the optical and redox characteristics.

Figure 5A shows the UV−vis absorption spectra of **1** and **2** in chloroform. Apparent from Figure 5A is that the two compounds exhibit similar electronic transitions and possess two major absorption bands: a set of small-wavelength absorption bands (from 300 to 500 nm) and a broad absorption band at longer wavelengths (from 600 to 800 nm). The longest wavelength absorption is red-shifted by 28 nm (0.05 eV) when moving from **2** (790 nm, 1.57 eV) to **1** (818 nm, 1.52 eV), which is attributed to the slightly more effective orbital delocalization between the aromatic bowl core and the ethynyl moieties in **1** (Table 2). Time-dependent DFT (TDDFT) calculations at the OT-LC-ωHPBE/cc-pVDZ +GD3 level of theory are consistent with these trends: The TDDFT $S_0 \rightarrow S_1$ for **1** (1.51 eV) is 0.06 eV smaller than that for **2** (1.57 eV), and in each case the transition is described as being predominantly HOMO → LUMO (Table S3); the

https://dx.doi.org/10.1021/jacs.9b12192
J. Am. Chem. Soc. 2020, 142, 2460−2470

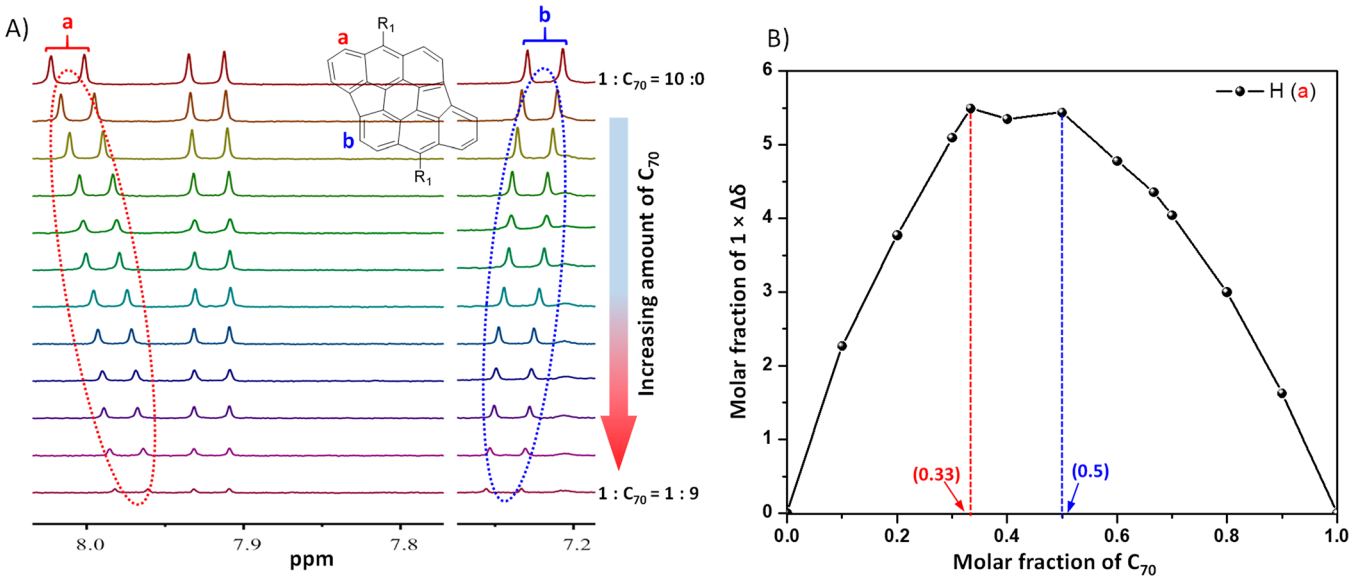

Figure 6. (A) ^{1}H NMR spectrum of **1** when titrated with C_{70} (the total concentration [**1**] + [C_{70}] = 6.0 × 10^{-4} M, toluene-d_8, 298 K) and (B) Job plot based on ^{1}H NMR titration of **1** with C_{70} in toluene-d_8. The chemical shift change [$\Delta\delta$] of proton a of **1** is used, and the mole fraction of C_{70} corresponds to [C_{70}]/[**1**] + [C_{70}].

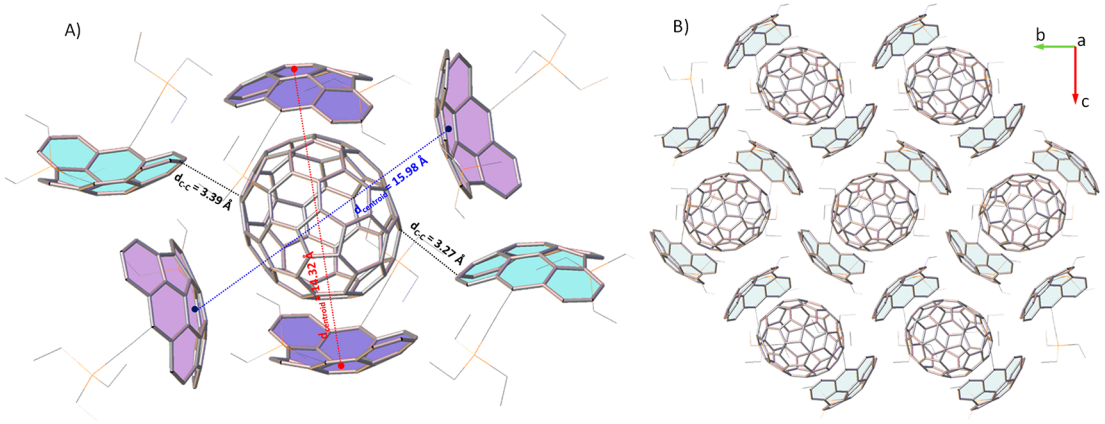

Figure 7. X-ray structure of **1**-C_{70}. For clarity, only one C_{70} disorder component is shown, and H atoms are omitted. (A) Selected intermolecular distances in **1**-C_{70} cocrystals and (B) crystal packing of **1**-C_{70}.

natural transition orbitals (NTO) derived for these transitions showcase similar trends (Figure S6).

The redox properties of **1** and **2** were examined by cyclic voltammetry (CV; 0.1 M $TBAPF_6$, 100 mV/s) in dichloromethane, with the onset oxidation−reduction potentials determined relative to Fc/Fc^+ (4.8 eV) (Figure 5B). The CVs of **1** and **2** exhibit two reversible reduction peaks, one reversible oxidation peak, and one irreversible oxidation peak, respectively. The first-wave reduction potential of **1** is −1.10 V, which is significantly more positive than that of **2** (−1.34 V), while their first-wave oxidation potentials are essentially comparable. According to these onset potentials, the electron affinities (EA) of **1** and **2** are estimated to be −3.76 and −3.55 eV, respectively, while the ionization potentials (IP) are estimated to be −5.15 and −5.16 eV, respectively. The differences in potential are consistent with the differences observed in the respective LUMO and HOMO energies, and DFT-computed adiabatic electron affinities (AEA) and ionization potentials (AIP; Table S2), and the corresponding radical-anion and radical-cation spin densities. Notably, the EA of **1** is close to other n-type materials, such as [6,6]-phenyl-C_{61}-butyric acid methyl ester ($PC_{60}BM$)[22] and perylene diimides.[23]

Assembly of 1 and 2 with C_{70}. Because of potential shape complementarity, **1** and **2** were postulated to be good partners to cocrystallize with C_{70}. Although the UV−vis spectra do not show evidence of interactions between C_{70} and either of these compounds in solution, the intermolecular interactions between **1** and C_{70} were confirmed by ^{1}H NMR. As shown in Figure 6A, adding C_{70} into a toluene-d_8 solution of **1**, the proton labeled *a* increasingly shifts upfield, while the proton labeled *b* increasingly shifts downfield, with increasing amounts of C_{70}. These results suggest that a **1**-C_{70} complex is being formed.[24] The Job plot based on the titration clearly indicates the 1:1 and 2:1 complex formation in toluene-d_8 solution (Figure 6B). On the basis of the proton shift values, the first and second binding constants (K_a) of **1** with C_{70} in toluene-d_8 at 298 K are estimated to be 1575 ± 17 and 1463 ± 51 M^{-1} (Figure S14).[25] In contrast, ^{1}H NMR titration experiments of **2** and C_{70} show no complexation-induced chemical shift (Figure S15). This is likely due to the steric hindrance of iso-

https://dx.doi.org/10.1021/jacs.9b12192
J. Am. Chem. Soc. 2020, 142, 2460−2470

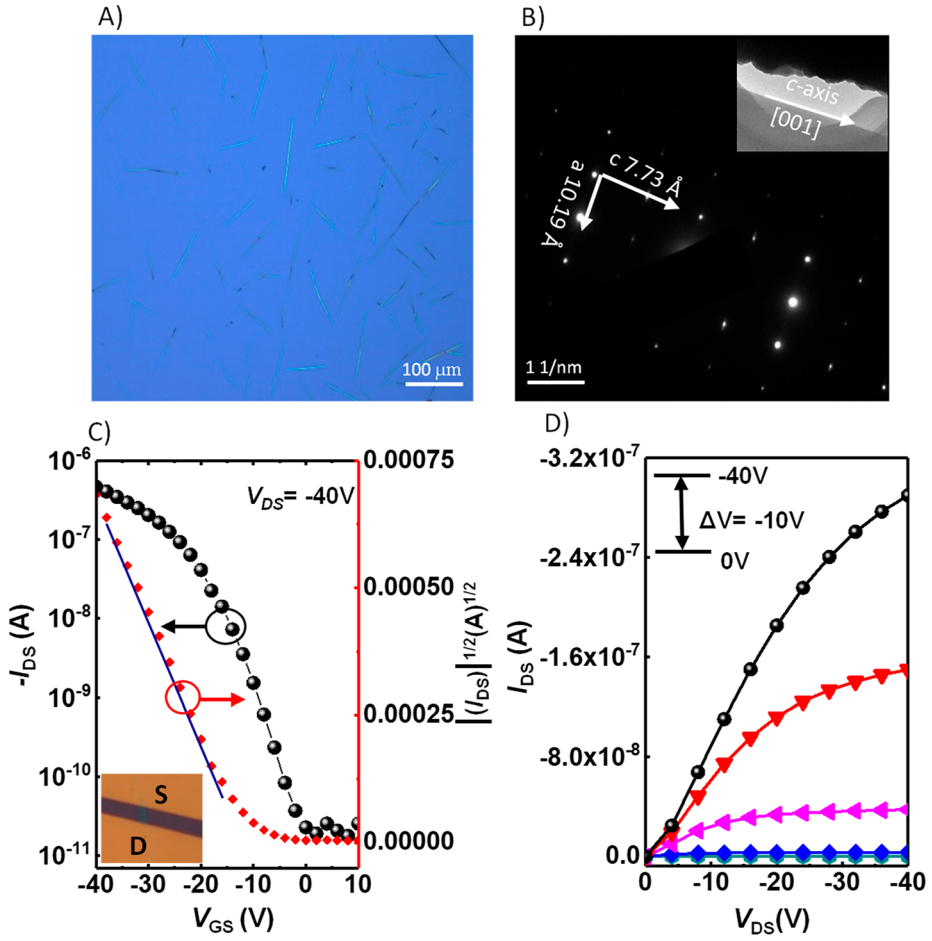

Figure 8. (A) Optical microscopy image of **1** microfibers from toluene solution, (B) the selected-area electron diffraction (SAED) patterns of microfibers of **1** (inset: TEM image of a single-crystalline microfiber), and (C) the transfer and (D) output characteristics of OFET device based on **1** single-crystalline microfiber (W/L = 2.1/5.6).

propyl groups that prevent the intermolecular interaction between the curved surfaces of **2** and C_{70}.

To gain further insight into the complex of **1** and C_{70}, **1**-C_{70} cocrystals suitable for X-ray diffraction analysis were grown by slow evaporation of *n*-butyl acetate solution with equimolar amounts of **1** and C_{70} at room temperature. The cocrystal crystallizes in the $P2_1/c$ space group with four molecules of **1** and two C_{70} molecules per unit cell. The crystallographic analysis reveals the formation of the complex with a 2:1 ratio. The centroid of the C_{70} molecule sits on a crystallographic inversion center, which forces the molecule to be disordered. The most satisfactory model required four disorder components, with the C_{70} molecule treated as a rigid body. As shown in Figure 7A, the C_{70} is embraced by two bowl compounds with multiple concave−convex interactions. The distance from the centroids of the six-membered rings of the two bowls is 14.32 Å. In addition, convex−convex interactions can be seen between the convex surfaces of **1** and C_{70} with a larger centroid distance of 15.98 Å. The C_{70} molecule further interacts with another adjacent bowl molecule through short C−C contacts. Therefore, each C_{70} molecule is in close contact with six bowl molecules, forming two-dimensional sheets with the C_{70} arranged linearly (Figure 7B).

Charge-Carrier Transport Properties. Although many buckybowls have the potential for self-assembly in the solid state via strong concave-in-convex interactions that can enable efficient charge-carrier transport through the curved π-surfaces, the functional groups at peripheral positions are usually too bulky to promote good π-packing motifs for efficient transport. Here, the TES-ethynyl group helps with the arrangement of the buckybowls with strong concave-in-convex interactions, which could favor charge-carrier transport through the curved π-surfaces. We evaluated the intrinsic charge-carrier mobilities of **1** and **1**-C_{70} complex through single-crystal organic field-effect transistors (SC-OFETs). SC-OFETs were fabricated by a "gold strips" technique on an octadecyltrichlorosilane (OTS) treated substrate (OTS-SiO_2/Si) with Au as electrodes.[26] As expected, **1** readily forms microfibers by slow evaporation of toluene solution (Figure 8A). The strong out-of-plane X-ray diffraction peaks indicate that the microfibers have high crystallinity (Figure S16), and the SAED patterns could be indexed on the basis of the single-crystal data, which indicate that the *c*-axis is the crystal-growth direction with strong concave−convex interactions (Figure 8B). Figure 8C and D represents the output and transfer characteristics of microfibers of **1** tested under ambient conditions. **1** shows exclusive p-type transport behavior with an average mobility up to 0.17 $cm^2\ V^{-1}\ s^{-1}$ and a maximum mobility of 0.31 $cm^2\ V^{-1}\ s^{-1}$. Note that the mobility of **1** is one of the highest values reported for buckybowls.[27] In contrast, its planar isomer derivative, triisopropylsilyl (TIPS)-functionalized bisanthene, behaves as an insulator even though it forms perfectly cofacial one-

https://dx.doi.org/10.1021/jacs.9b12192
J. Am. Chem. Soc. 2020, 142, 2460−2470

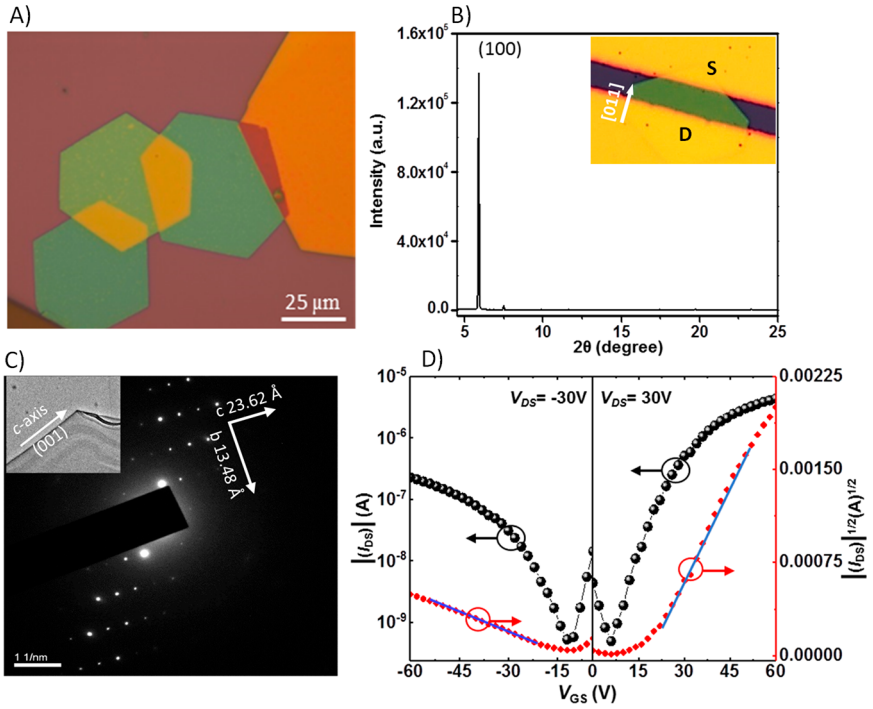

Figure 9. (A) Optical microscopy image of single-crystalline microplates of **1**-C_{70}; (B) XRD pattern of **1**-C_{70} cocrystals (inset: optical microscopy image of the single-crystal transistor with electrodes to probe the charge transport along the [011] direction); (C) the selected-area electron diffraction (SAED) patterns of microplates of **1**-C_{70}; and (D) the transfer characteristic of OFET device based on **1**-C_{70} cocrystal (W/L = 12.1/7.2).

dimensional $\pi-\pi$ stacking arrangements.[28] We note that evaluations of the intermolecular electronic couplings based on the bulk crystal structure along the bowl−bowl stacking directions via the fragment-orbital approach[29] at the OT-LC-ωHPBE/cc-pVDZ+GD3 level of theory reveal HOMO:HOMO couplings of 15 meV; interestingly, the LUMO:LUMO couplings are twice as large at 34 meV (Figure S9 and Table S4).

1-C_{70} cocrystals were prepared by slow evaporation of *n*-butyl acetate solution. Figure 9A shows the optical microscopy image of the cocrystals, which form hexagonal plates. The cocrystals exhibit a strong Bragg reflection, which could be indexed as [100] according to the crystallographic data for the bulk crystal (Figure 9B). The *d*-spacing (15.01 Å) calculated from the first peak is almost identical to the length of the *a*-axis observed in the single-crystal structure, which indicates the crystals grow with the *bc* plane parallel to the substrate. Notably, there is no diffraction peak for C_{70} or **1** observed. Furthermore, the transmission electron microscopy (TEM) image of an individual nanoribbon and its corresponding selected area electron diffraction (SAED) patterns show ordered and bright diffractions, indicating the high quality of the cocrystals (Figure 9C). The SAED patterns of the cocrystals could be also indexed on the basis of the single-crystal data, which further confirm that the *bc* plane of the crystal is parallel to the surface of the substrate. Figure 9D represents the transfer characteristics of cocrystals tested under nitrogen. The cocrystals show ambipolar characteristics, with average electron and hole mobilities of 0.20 and 0.03 $cm^2\ V^{-1}\ s^{-1}$, respectively, and maximum electron and hole mobilities of 0.40 and 0.07 $cm^2\ V^{-1}\ s^{-1}$, respectively, along the [011] direction (Table S8). We note that the hole mobility of the cocrystal is 3−6 times smaller than that of pure **1**, while the electron mobility is the highest value previously reported for a C_{70}-containing material. The fragment-orbital approach was again used to evaluate the electronic couplings among **1** and C_{70} in the cocrystal (Figure S10); note that unit cells were too large for evaluation of the full band structure. It is interesting that the LUMOs of **1** (−2.14 eV) and C_{70} (−2.30 eV) are energetically close. Depending on the pathway followed in the crystal, the LUMO:LUMO couplings among the **1** and C_{70} ranged from 10 to 45 meV, while the HOMO:HOMO couplings ranged from 7 to 52 meV (with one pathway near 0 meV) (Table S5). We attempted to determine the superexchange electronic coupling among the bowls (through a C_{70}) or the C_{70} (through a bowl) through the energy-splitting-in-dimer approach (ESDA) at the OT-LC-ωHPBE/cc-pVDZ+GD3 level of theory, as superexchange is an established mechanism in donor−acceptor cocrystals;[30] here, we assumed that holes are transported among the bowls and electrons are transported among the C_{70}. For holes, there is one pathway with a superexchange electronic coupling of 10 meV. For the C_{70}, superexchange electronic couplings are small to negligible. In general, the combination of the strategically modified buckybowl with its perfect shape complementary toward fullerene provides a powerful route to achieve organic complexes with tunable crystal packing and transport behavior.

CONCLUSION

In summary, we described the synthesis and characterization of a novel C_{70} subunit substituted with TES-ethynyl and 2,4,6-triisopropylphenyl groups at the *meta*-positions, using the palladium-catalyzed intramolecular C−H arylation of chlorinated dibenzo[*a*,*j*]perylenes. A comparative study of the resulting two compounds (**1** and **2**) indicates that the substituents play an essential role regarding the optical and

https://dx.doi.org/10.1021/jacs.9b12192
J. Am. Chem. Soc. 2020, 142, 2460−2470

electrochemical properties, aromaticity, and crystal packing. The single-crystal X-ray analysis shows that the TES-ethynyl substituent in **1** leads to the enhancement of bond length alternation, resulting in weak aromaticity of the six-membered rings of the buckybowl skeleton. As compared to that of **2**, the longest absorption of **1** is red-shifted by 28 nm and the EA is more negative by 0.21 eV; these results are an effect of the extended conjugation from the buckybowl onto the ethynyl moieties. Further, **1** shows a one-dimensional (1D) concave-in-convex stacking motif, which displays a hole mobility of 0.31 $cm^2\ V^{-1}\ s^{-1}$. In particular, **1** serves as electron donor to encapsulate C_{70}, leading to two-dimensional cocrystals, which exhibit ambipolar transport characteristics with electron and hole mobilities up to 0.40 and 0.07 $cm^2\ V^{-1}\ s^{-1}$. This is the first device application of functionalized C_{70} fragment, which highlights the high potential of buckybowls for the development of novel semiconductors for organic devices as well as for future development in solution-phase fullerene chemistry.

■ ASSOCIATED CONTENT

Supporting Information

The Supporting Information is available free of charge at https://pubs.acs.org/doi/10.1021/jacs.9b12192.

Detailed synthesis and characterization of the compounds; ^1H NMR, ^{13}C NMR, $^1H-^1H$ COSY, and HRMS spectra of the compounds; NMR titration and variable-temperature NMR studies; crystal data for **1**, **2**, **5**, **8**, and **1**-C_{70}; UV and CV measurements; theoretical calculation details; and device fabrication and characterization (PDF)

X-ray crystallographic data for compound **1** (CIF)

X-ray crystallographic data for compound **2** (CIF)

X-ray crystallographic data for compound **5** (CIF)

X-ray crystallographic data for compound **8** (CIF)

X-ray crystallographic data for compound **1**-C_{70} (CIF)

■ AUTHOR INFORMATION

Corresponding Author

Lei Zhang − *Beijing University of Chemical Technology, Beijing, People's Republic of China;* orcid.org/0000-0002-0162-7222; Email: zhl@mail.buct.edu.cn

Other Authors

Guangpeng Gao − *Beijing University of Chemical Technology, Beijing, People's Republic of China*

Meng Chen − *Beijing University of Chemical Technology, Beijing, People's Republic of China*

Josiah Roberts − *University of Kentucky, Lexington, Kentucky*

Meng Feng − *Beijing University of Chemical Technology, Beijing, People's Republic of China*

Chengyi Xiao − *Beijing University of Chemical Technology, Beijing, People's Republic of China;* orcid.org/0000-0002-7253-7136

Guowei Zhang − *Beijing University of Chemical Technology, Beijing, People's Republic of China*

Sean Parkin − *University of Kentucky, Lexington, Kentucky*

Chad Risko − *University of Kentucky, Lexington, Kentucky;* orcid.org/0000-0001-9838-5233

Complete contact information is available at: https://pubs.acs.org/10.1021/jacs.9b12192

Author Contributions

[⊥]G.G. and M.C. contributed equally.

Notes

The authors declare no competing financial interest.

■ ACKNOWLEDGMENTS

L.Z. thanks the National Science Foundation of China (NSFC) (21672020) and the Beijing Natural Science Foundation (2182049). G.G. thanks the Fundamental Research Funds for the Central Universities (ZY1904) and the China Postdoctoral Science Foundation (2018M641159). S.P. thanks the NSF MRI program (grants CHE-031916 and CHE-162532). C.R. acknowledges funding from the National Science Foundation Designing Materials to Revolutionize and Engineer our Future (NSF DMREF) program under award DMR-1627428. Supercomputing resources on the Lipscomb High Performance Computing Cluster were provided by the University of Kentucky Information Technology Department and Center for Computational Sciences (CCS).

■ REFERENCES

(1) (a) Wu, Y.; Siegel, J. S. Aromatic Molecular-Bowl Hydrocarbons: Synthetic Derivatives, Their Structures, and Physical Properties. *Chem. Rev.* **2006**, *106*, 4843−4867. (b) *Fragments of Fullerenes and Carbon Nanotubes: Designed Synthesis, Unusual Reactions, and Coordination Chemistry*; Petrukhina, M. A., Scott, L. T., Eds.; Wiley-VCH: Weinheim, Germany, 2011. (c) Tsefrikas, V. M.; Scott, L. T. Geodesic Polyarenes by Flash Vacuum Pyrolysis. *Chem. Rev.* **2006**, *106*, 4868−4884. (d) Wu, Y.; Siegel, J. S. Synthesis, Structures, and Physical Properties of Aromatic Molecular-Bowl Hydrocarbons. *Top. Curr. Chem.* **2014**, *349*, 63−120.

(2) (a) Li, X.; Li, X.; Kang, F.; Inagaki, M. Buckybowls: Corannulene and Its Derivatives. *Small* **2016**, *12*, 3206−3223. (b) Eleni Nestoros, E.; Stuparu, C. M. Corannulene: A Molecular Bowl of Carbon with Multifaceted Properties and Diverse Applications. *Chem. Commun.* **2018**, *54*, 6503−6519. (c) Saito, M.; Shinokubo, H.; Sakurai, H. Figuration of Bowl−Shaped π-Conjugated Molecules: Properties and Functions. *Mater. Chem. Front.* **2018**, *2*, 635−661. (d) Baldridge, K. K.; Siegel, J. S. Canastanes: Ab Initio Quantum Mechanical Prediction of New Curved Polynuclear Aromatic Hydrocarbon Motif. *J. Am. Chem. Soc.* **1999**, *121*, 5332−5333. (e) Tan, Q.; Higashibayashi, S.; Karanjit, S.; Sakurai, H. Enantioselective Synthesis of a Chiral Nitrogendoped Nuckybowl. *Nat. Commun.* **2012**, *3*, 891.

(3) (a) Amaya, T.; Seki, S.; Moriuchi, T.; Nakamoto, K.; Nakata, T.; Sakane, H.; Saeki, A.; Tagawa, S.; Hirao, T. Anisotropic Electron Transport Properties in Sumanene Crystal. *J. Am. Chem. Soc.* **2009**, *131*, 408−409. (b) Ayalon, A.; Rabinovitz, M.; Cheng, P.; Scott, L. T. Corannulene Tetraanion: A Novel Species with Concentric Anionic Rings. *Angew. Chem., Int. Ed. Engl.* **1992**, *31*, 1636−1637. (c) Shi, K.; Lei, T.; Wang, X.; Wang, J.; Pei, J. A Bowl-Shaped Molecule for Organic Field-Effect Transistors: Crystal Engineering and Charge Transport Switching by Oxygen Doping. *Chem. Sci.* **2014**, *5*, 1041−1045. (d) Chen, R.; Lu, R.; Shi, K.; Wu, F.; Fang, H.; Niu, Z.; Yan, X.; Luo, M.; Wang, X.; Yang, C.; Wang, X.; Xu, B.; Xia, H.; Pei, J.; Cao, X. Corannulene Derivatives with Low LUMO Levels and Dense Convex-Concave Packing for n-Channel Organic Field-Effect Transistors. *Chem. Commun.* **2015**, *51*, 13768−13771. (e) Lu, R.; Zhou, Y.; Yan, X.; Shi, K.; Zheng, Y.; Luo, M.; Wang, X.; Pei, J.; Xia, H.; Zoppi, L.; Baldridge, K. K.; Siegel, J. S.; Cao, X. Thiophene-Fused Bowl-Shaped Polycyclic Aromatics with A Dibenzo[*a, g*]corannulene Core for Organic Field-Effect Transistors. *Chem. Commun.* **2015**, *51*, 1681−1684.

(4) (a) Haupt, A.; Lentz, D. Corannulenes with Electron-Withdrawing Substituents: Synthetic Approaches and Resulting Structural and Electronic Properties. *Chem. - Eur. J.* **2019**, *25*, 3440−3454. (b) Schmidt, B. M.; Seki, S.; Topolinski, B.; Ohkubo, K.; Fukuzumi, S.; Sakurai, H.; Dieter, L. Electronic Properties of Trifluoromethylated Corannulenes. *Angew. Chem., Int. Ed.* **2012**, *51*, 11385−11388. (c) Kuvychko, I. V.; Spisak, S. N.; Chen, Y.; Popov, A. A.; Petrukhina, M. A.; Strauss, S. H.; Boltalina, O. V. A Buckybowl with a Lot of Potential: C_5-$C_{20}H_5(CF_3)_5$. *Angew. Chem., Int. Ed.* **2012**, *51*, 4939−4942.

(5) (a) Lampart, S.; Roch, L. M.; Dutta, A. K.; Wang, Y.; Warshamanage, R.; Finke, A. D.; Linden, A.; Baldridge, K. K.; Siegel, J. S. Pentaindenocorannulene: Properties, Assemblies, and C_{60} Complex. *Angew. Chem., Int. Ed.* **2016**, *55*, 14648−14652. (b) Lu, R.; Wu, S.; Bao, Y.; Yang, L.; Qu, H.; Saha, M.; Wang, X.; Zhuo, Y.; Xu, B.; Pei, J.; Zhang, H.; Weng, W.; Cao, X. Cocrystallization of Imide-Fused Corannulene Derivatives and C_{60}:Guest-Induced Conformational Switching and 1:1 Segregated Packing. *Chem. - Asian J.* **2018**, *13*, 2934−2938. (c) Dawe, L. N.; AlHujran, T. A.; Tran, H.; Mercer, J. I.; Jackson, E. A.; Scott, L. T.; Georghiou, P. E. Corannulene and Its Penta-*tert*-butyl Derivative Co-crystallize 1:1 with Pristine C_{60}-Fullerene. *Chem. Commun.* **2012**, *48*, 5563−5565. (d) Shoji, Y.; Kajitani, K.; Ishiwari, F.; Ding, Q.; Sato, H.; Anetai, H.; Akutagawa, T.; Sakuraif, H.; Fukushima, T. Hexathioalkyl Sumanenes: an Electron-Donating Buckybowl as a Building Block for Supramolecular Materials. *Chem. Sci.* **2017**, *8*, 8405−8410. (e) Filatov, A. S.; Ferguson, M. V.; Spisak, S. N.; Li, B.; Campana, C. F.; Petrukhina, M. A. Bowl-Shaped Polyarenes as Concave-Convex Shape Complementary Hosts for C_{60}- and C_{70}-Fullerenes. *Cryst. Growth Des.* **2014**, *14*, 756−762. (f) Yokoi, H.; Hiraoka, Y.; Hiroto, S.; Sakamaki, D.; Seki, S.; Shinokubo, H. Nitrogen-Embedded Buckybowl and Its Assembly with C_{60}. *Nat. Commun.* **2015**, *6*, 8215. (g) Pérez, E. M.; Martín, N. π-π interactions in carbon nanostructures. *Chem. Soc. Rev.* **2015**, *44*, 6425−6433. (h) David Canevet, D., Dr.; Pérez, E. M.; Martín, N. Wraparound Hosts for Fullerenes: Tailored Macrocycles and Cages. *Angew. Chem., Int. Ed.* **2011**, *50*, 9248−9259.

(6) Wang, Y.; Li, Y.; Zhu, W.; Liu, J.; Zhang, X.; Li, R.; Zhen, Y.; Dong, H.; Hu, W. Co-crystal Engineering: a Novel Method to Obtain One-Dimensional (1D) Carbon Nanocrystals of Corannulene-Fullerene by a Solution Process. *Nanoscale* **2016**, *8*, 14920−14924.

(7) Ball, M.; Zhong, Y.; Wu, Y.; Schenck, C.; Ng, F.; Steigerwald, M.; Xiao, S.; Nuckolls, C. Contorted Polycyclic Aromatics. *Acc. Chem. Res.* **2015**, *48*, 267−276.

(8) (a) Feng, C.-N.; Hsieh, Y.-C.; Wu, Y.-T. Metal-Catalyzed Cascade Reactions: Useful Synthetic Tools for the Preparation of Polycyclic Arenes. *Chem. Rec.* **2015**, *15*, 266−279.

(9) (a) Reisch, H. A.; Bratcher, M. S.; Scott, L. T. Imposing Curvature on a Polyarene by Intramolecular Palladium-Catalyzed Arylation Reactions: A Simple Synthesis of Dibenzo[*a, g*]corannulene. *Org. Lett.* **2000**, *2*, 1427−1430. (b) Marcinow, Z.; Sygula, A.; Ellern, A.; Rabideau, P. W. Lowering Inversion Barriers of Buckybowls by Benzannelation of the Rim: Synthesis and Crystal and Molecular Structure of 1,2-Dihydrocyclopenta[*b, c*]dibenzo[*g, m*]corannulene. *Org. Lett.* **2001**, *3*, 3527−3529.

(10) (a) Jin, T.; Zhao, J.; Asao, N.; Yamamoto, Y. Metal-Catalyzed Annulation Reactions for π-Conjugated Polycycles. *Chem. - Eur. J.* **2014**, *20*, 3554−3576. (b) Whalley, A. C.; Plunkett, K. N.; Gorodetsky, A. A.; Schenck, C. L.; Chiu, C.-Y.; Steigerwald, M. L.; Nuckolls, C. Bending Contorted Hexabenzocoronene into ABowl. *Chem. Sci.* **2011**, *2*, 132−135.

(11) (a) Wegner, H. A.; Reisch, H.; Rauch, K.; Demeter, A.; Zachariasse, K. A.; de Meijere, A.; Scott, L. T. Oligoindenopyrenes: A New Class of Polycyclic Aromatics. *J. Org. Chem.* **2006**, *71*, 9080−9087. (b) Jackson, E. A.; Steinberg, B. D.; Bancu, M.; Wakamiya, A.; Scott, L. T. Pentaindenocorannulene and Tetraindenocorannulene: New Aromatic Hydrocarbon π Systems with Curvatures Surpassing That of C_{60}. *J. Am. Chem. Soc.* **2007**, *129*, 484−485. (c) Steinberg, B. D.; Jackson, E. A.; Filatov, A. S.; Wakamiya, A.; Petrukhina, M. A.; Scott, L. T. Aromatic π-Systems More Curved Than C_{60}. The Complete Family of All Indenocorannulenes Synthesized by Iterative Microwave-Assisted Intramolecular Arylations. *J. Am. Chem. Soc.* **2009**, *131*, 10537−10545.

(12) Liu, J.; Osella, S.; Ma, J.; Berger, R.; Beljonne, D.; Schollmeyer, D.; Feng, X.; Müllen, K. Fused Dibenzo[*a, m*]rubicene: A New Bowl-Shaped Subunit of C_{70} Containing Two Pentagons. *J. Am. Chem. Soc.* **2016**, *138*, 8364−8367.

(13) (a) Wu, T.-C.; Chen, M.-K.; Lee, Y.-W.; Kuo, M.-Y.; Wu, Y.-T. Bowl-Shaped Fragments of C_{70} or Higher Fullerenes: Synthesis, Structural Analysis, and Inversion Dynamics. *Angew. Chem., Int. Ed.* **2013**, *52*, 1289−1293. (b) Chang, H.-I.; Huang, H.-T.; Huang, C.-H.; Kuo, M.-Y.; Wu, Y. T. Diindeno[1,2,3,4-*defg*; 4′,3′,2′,1′-*mnop*]-chrysenes: Solution-Phase Synthesis and the Bowl-to-Bowl Inversion Barrier. *Chem. Commun.* **2010**, *46*, 7241−7243. (c) Chen, M.-K.; Hsin, H.-J.; Wu, T.-C.; Kang, B.-Y.; Lee, Y.-W.; Kuo, M.-K.; Wu, Y.-T. Highly Curved Bowl-Shaped Fragments of Fullerenes: Synthesis, Structural Analysis, and Physical Properties. *Chem. - Eur. J.* **2014**, *20*, 598−608.

(14) (a) Hishikawa, S.; Okabe, Y.; Tsuruoka, R.; Higashibayashi, S.; Ohtsu, H.; Kawano, M.; Yakiyama, Y.; Sakurai, H. Synthesis of a C_{70} Fragment Buckybowl $C_{28}H_{14}$ from a C_{60} Fragment Sumanene. *Chem. Lett.* **2017**, *46*, 1556−1559. (b) Huang, J.-L.; Rao, B.; Kumar, M. P.; Lu, H.-F.; Chao, I.; Lin, C.-H. Dicyclopenta[*ghi,pqr*]perylene as a Structural Motif for Bowl-Shaped Hydrocarbons: Synthetic and Conformational Studies. *Org. Lett.* **2019**, *21*, 2504−2508.

(15) Wood, J. D.; Jellison, J. L.; Finke, A. D.; Wang, L.; Plunkett, K. N. Electron Acceptors Based on Functionalizable Cyclopenta[*hi*]-aceanthrylenes and Dicyclopenta[*de,mn*]tetracenes. *J. Am. Chem. Soc.* **2012**, *134*, 15783−15789.

(16) Thilgen, C.; Herrmann, A.; Diederich, F. The Covalent Chemistry of Higher Fullerenes: C_{70} and Beyond. *Angew. Chem., Int. Ed. Engl.* **1997**, *36*, 2268−2280.

(17) Petrukhina, M. A.; Andreini, K. W.; Mack, J.; Scott, L. T. X-ray Quality Geometries of Geodesic Polyarenes from Theoretical Calculations: What Levels of Theory Are Reliable? *J. Org. Chem.* **2005**, *70*, 5713−5716.

(18) Zou, Y.; Zeng, W.; Gopalakrishna, T. Y.; Han, Y.; Jiang, Q.; Wu, J. Dicyclopenta[4,3,2,1-*ghi*:4′,3′,2′,1′-*pqr*]perylene: A Bowl-Shaped Fragment of Fullerene C_{70} with Global Antiaromaticity. *J. Am. Chem. Soc.* **2019**, *141*, 7266−7270.

(19) Krygowski, T. M.; Cyrański, M. K. Structural Aspects of Aromaticity. *Chem. Rev.* **2001**, *101*, 1385−1419.

(20) Gasparro, F. P.; Kolodny, N. H. NMR Determination of the Rotational Barrier in *N,N*-Dimethylacetamide. *J. Chem. Educ.* **1977**, *54*, 258−261.

(21) Frisch, M. J.; Trucks, G. W.; Schlegel, H. B.; Scuseria, G. E.; Robb, M. A.; Cheeseman, J. R.; Scalmani, G.; Barone, V.; Petersson, G. A.; Nakatsuji, H.; Li, X.; Caricato, M.; Marenich, A. V.; Bloino, J.; Janesko, B. G.; Gomperts, R.; Mennucci, M.; Hratchian, H. P.; Ortiz, J. V.; Izmaylov, A. F.; Sonnenberg, J. L.; Williams-Young, D.; Ding, F.; Lipparini, F.; Egidi, F.; Goings, J.; Peng, B.; Petrone, A.; Henderson, T.; Ranasinghe, D.; Zakrzewski, V. G.; Gao, J.; Rega, N.; Zheng, G.; Liang, W.; Hada, M.; Ehara, M.; Toyota, K.; Fukuda, R.; Hasegawa, J.; Ishida, M.; Nakajima, T.; Honda, Y.; Kitao, O.; Nakai, H.; Vreven, T.; Throssell, K.; Montgomery, J. A.; Peralta, J. E., Jr.; Ogliaro, F.; Bearpark, M. J.; Heyd, J. J.; Brothers, E. N.; Kudin, K. N.; Staroverov, V. N.; Keith, T. A.; Kobayashi, R.; Normand, J.; Raghavachari, K.; Rendell, A. P.; Burant, J. C.; Iyengar, S. S.; Tomasi, J.; Cossi, M.; Millam, J. M.; Klene, M.; Adamo, C.; Cammi, R.; Ochterski, J. W.; Martin, R. L.; Morokuma, K.; Farkas, O.; Foresman, J. B.; Fox, D. J. *Gaussian 16*, revision C.01; Gaussian, Inc.: Wallingford, CT, 2016.

(22) Liu, T.; Troisi, A. What Makes Fullerene Acceptors Special as Electron Acceptors in Organic Solar Cells and How to Replace Them. *Adv. Mater.* **2013**, *25*, 1038−1041.

(23) (a) Jiang, W.; Li, Y.; Wang, Z. Tailor-Made Rylene Arrays for High Performance n-Channel Semiconductors. *Acc. Chem. Res.* **2014**, *47*, 3135−3147. (b) Chen, L.; Li, C.; Müllen, K. Beyond Perylene Diimides: Synthesis, Assembly and Function of Higher Rylene Chromophores. *J. Mater. Chem. C* **2014**, *2*, 1938−1956.

https://dx.doi.org/10.1021/jacs.9b12192
J. Am. Chem. Soc. 2020, 142, 2460−2470

(24) (a) Zhou, Z. M.; Qin, Y. K.; Xu, W.; Zhu, D. B. Supramolecular Association Behavior of a Strong C_{60} Receptor with Conjugated Pentacene and Tetrathiafulvalene Moieties in Solution and in the Solid State. *Chem. Commun.* **2014**, *50*, 4082−4084. (b) Lu, X.; Gopalakrishna, T. Y.; Han, Y.; Ni, Y.; Zou, Y.; Wu, J. Bowl-Shaped Carbon Nanobelts Showing Size-Dependent Properties and Selective Encapsulation of C_{70}. *J. Am. Chem. Soc.* **2019**, *141*, 5934−5941.
(25) (a) Yamamoto, Y.; Tsurumaki, E.; Wakamatsu, K.; Toyota, S. Nan0-Saturn: Experimental Evidence of Complex Formation of an Anthrance Cyclic Ring with C_{60}. *Angew. Chem., Int. Ed.* **2018**, *57*, 8199−8202. (b) Tokimaru, Y.; Ito, S.; Nozaki, K. A Hybrid of Corannulene and Azacorannulene: Synthesis of a Highly Curved Nitrogen-Containing Buckybowl. *Angew. Chem., Int. Ed.* **2018**, *57*, 9818−9822.
(26) Tang, Q.; Tong, Y. H.; Li, H. X.; Zhu, Y.; Li, Q. L.; Hu, W.; Liu, Y.; Zhu, D. High-Performance Air-Stable Bipolar Field-Effect Transistors of Organic Single-Crystalline Ribbons with an Air-Gap Dielectric. *Adv. Mater.* **2008**, *20*, 1511−1515.
(27) Fu, B.; Hou, X.; Wang, C.; Wang, Y.; Zhang, X.; Li, R.; Shao, X.; Hu, W. A Bowl-Shaped Sumanene Derivative with Dense Convex-Concave Columnar Packing for High Performance Organic Field-Effect Transistors. *Chem. Commun.* **2017**, *53*, 11407−11409.
(28) (a) Zhang, L.; Fonari, A.; Zhang, Y.; Zhao, G.; Coropceanu, V.; Hu, W.; Parkin, S.; Brédas, J.-L.; Briseno, A. L. Triisopropylsilylethynyl-Functionalized Graphene-Like Fragment Semiconductors: Synthesis, Crystal Packing, and Density Functional Theory Calculations. *Chem. - Eur. J.* **2013**, *19*, 17907−17916. (b) Zhang, L.; Cao, Y.; Colella, N. S.; Liang, Y.; Brédas, J.-L.; Houk, K. N.; Briseno, A. L. Unconventional, Chemically Stable, and Soluble Two-Dimensional Angular Polycyclic Aromatic Hydrocarbons: From Molecular Design to Device Applications. *Acc. Chem. Res.* **2015**, *48*, 500−509.
(29) (a) Valeev, E. F.; Coropceanu, V.; da Silva Filho, D. A.; Salman, S.; Brédas, J.-L. Effect of Electronic Polarization on Charge-Transport Parameters in Molecular Organic Semiconductors. *J. Am. Chem. Soc.* **2006**, *128*, 9882−9886. (b) Coropceanu, V.; Cornil, J.; da Silva Filho, D. A.; Olivier, Y.; Silbey, R.; Brédas, J.-L. Charge Transport in Organic Semiconductors. *Chem. Rev.* **2007**, *107*, 926−952.
(30) (a) Zhu, L.; Yi, Y.; Li, Y.; Kim, E.-G.; Coropceanu, V.; Brédas, J.-L. Prediction of Remarkable Ambipolar Charge-Transport Characteristics in Organic Mixed-Stack Charge-Transfer Crystals. *J. Am. Chem. Soc.* **2012**, *134*, 2340−2347. (b) Qin, Y.; Zhang, J.; Zheng, X.; Geng, H.; Zhao, G.; Xu, W.; Hu, W.; Shuai, Z.; Zhu, D. Charge-Transfer Complex Crystal Based on Extended-π-Conjugated Acceptor and Sulfur-Bridged Annulene: Charge-Transfer Interaction and Remarkable High Ambipolar Transport Characteristics. *Adv. Mater.* **2014**, *26*, 4093−4099. (c) Zhang, J.; Gu, P.; Long, G.; Ganguly, R.; Li, Y.; Aratani, N.; Yamada, H.; Zhang, Q. Switching Charge-Transfer Characteristics from p-Type to n-Type Through Molecular "Doping" (Cocrystallization). *Chem. Sci.* **2016**, *7*, 3851−3856.

https://dx.doi.org/10.1021/jacs.9b12192
J. Am. Chem. Soc. 2020, 142, 2460−2470